Reconciling the Relationship Between the AMOC and Labrador Sea in OSNAP Observations and Climate Models

Matthew B Menary, Laura C Jackson, M. Susan Susan Lozier

Geophysical Research Letters

RESEARCH LETTER
10.1029/2020GL089793

Reconciling the Relationship Between the AMOC and Labrador Sea in OSNAP Observations and Climate Models

Matthew B. Menary[1], **Laura C. Jackson**[2], **and M. Susan Lozier**[3]

[1]LOCEAN/IPSL, Sorbonne Universités (SU)-CNRS-IRD-MNHN, Paris, France, [2]Met Office Hadley Centre, Met Office, Exeter, UK, [3]Earth and Atmospheric Sciences, Georgia Institute of Technology, Atlanta, GA, USA

Abstract The AMOC (Atlantic Meridional Overturning Circulation) is a key driver of climate variability. Our understanding, based largely on climate models, is that the Labrador Sea has an important role in shaping the evolution of the AMOC. However, a recent high-profile observational campaign (Overturning in the Subpolar North Atlantic, OSNAP) has called into question the importance of the Labrador Sea, and hence the credibility of the AMOC representation in climate models. Here, we attempt to reconcile these viewpoints by making the first direct comparison between OSNAP and a coupled climate model. The model compares well to the observations, demonstrating a more prominent role for overturning in the eastern than western subpolar gyre. Density anomalies generated by surface forcing in the Irminger Sea propagate into the Labrador Sea, where they dominate the density variability. Thus, the Labrador Sea may not be the origin of AMOC variability despite correlations with densities there.

Key Points:
- A coupled climate model shows agreement with recent observations (OSNAP), displaying a prominent role for the eastern subpolar gyre
- This model also demonstrates a link between AMOC and Labrador Sea densities, consistent with previous modeling-based paradigms
- In our model, this link arises as Labrador Sea density anomalies originate via surface forcing upstream in the Irminger Sea

Supporting Information:
- Supporting Information S1

Correspondence to:
M. B. Menary,
matthew.menary@locean.ipsl.fr

Citation:
Menary, M. B., Jackson, L. C., & Lozier, M. S. (2020). Reconciling the relationship between the AMOC and Labrador Sea in OSNAP observations and climate models. *Geophysical Research Letters*, *47*, e2020GL089793. https://doi.org/10.1029/2020GL089793

Received 16 JUL 2020
Accepted 1 SEP 2020
Accepted article online 9 SEP 2020

1. Introduction

The Atlantic Meridional Overturning Circulation (AMOC) is a key player in global climate through its meridional heat transport and ability to sequester anthropogenic carbon in the deep ocean (Buckley & Marshall, 2016). According to paleorecords and experiments with a wide variety of simple to complex climate models, it may be sensitive to changes in the climate, such as global warming and ice melt (freshening) from Greenland and the Arctic (Gregory et al., 2005; Stommel, 1961; Stouffer et al., 2006; Thornalley et al., 2018; Wood et al., 1999). It may also be predictable on decadal timescales (Robson et al., 2018), which would be valuable given the potential relationship between the AMOC and North Atlantic sea surface temperatures (Rahmstorf et al., 2015; Zhang & Wang, 2013) as well as the climate impacts of a shutdown of this circulation (Jackson et al., 2015).

It is almost always the case in climate models that there is a strong link between density in the northern subpolar gyre (SPG) and in the AMOC throughout the North Atlantic on long enough timescales (Roberts et al., 2013; Robson et al., 2016). In many models, this relationship is dominated by variability in the Labrador Sea (Guemas & Salas-Mélia, 2008; Medhaug et al., 2012; Menary et al., 2015). In these models, there is also usually strong (often overly vigorous) deep convection in the central Labrador Sea (as diagnosed by March mixed layer depths, MLDs) (Heuzé, 2017; Li et al., 2019). In other models, variability in convection in the eastern SPG or in the Greenland-Iceland-Norwegian (GIN) Seas dominates (Escudier et al., 2013; Park & Latif, 2010) and there is often relatively little wintertime deep convection in the Labrador Sea, at odds with direct observations that show deep, albeit sporadic, convection in this region (Yashayaev & Loder, 2016). It also remains unclear how convection (which involves no net vertical motion) is linked with vertical sinking (Pickart & Spall, 2007), and whether density anomalies that result from convection are propagated southward (Hodson & Sutton, 2012) or appear meridionally coherent due to common forcing (Zou et al., 2019). Furthermore, despite the model-derived paradigm of a strong link between convection, density, and overturning (generally in depth space) in the Labrador Sea and the AMOC throughout the North Atlantic, the precise mechanisms linking these processes may be dependent on model biases and resolution (Katsman et al., 2018; Menary & Hermanson, 2018; Menary et al., 2015).

From an observational viewpoint, the recent Overturning in the Subpolar North Atlantic Program (OSNAP) (Lozier et al., 2019) has shown that the overturning in the Labrador Sea is much smaller than that in the eastern SPG, both in the mean state and monthly variability. Other observational studies have found that

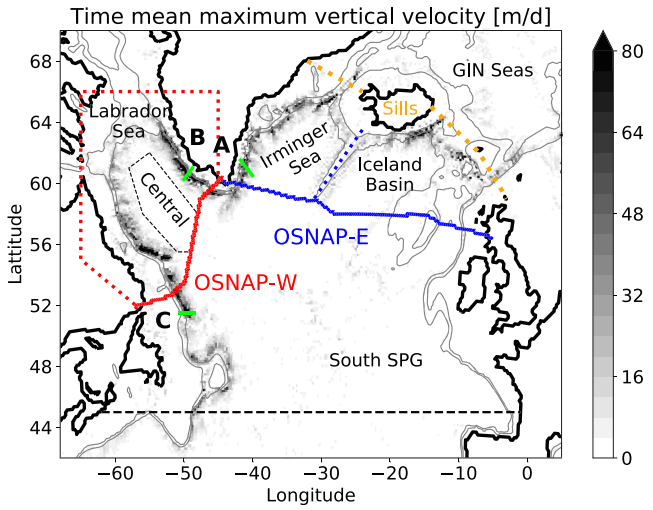

Figure 1. Absolute maxima from monthly mean vertical velocities (m/day) in the climate model throughout the water column (in depth space). The 500 and 1500 m isobaths are highlighted in gray. Also shown are key regions of interest for this study, including the OSNAP-E (blue) and OSNAP-W (red) sections and the location of the northern subpolar gyre overflow sills (yellow). Area averages are taken in the Labrador Sea (as bounded by OSNAP-W and the dashed red line); the Central Labrador Sea (bounded by the black dashed line); the Irminger Sea (bounded by OSNAP-E, the sills, and the dashed blue line); the eastern SPG (bounded by the sills and OSNAP-E); the GIN Seas (bounded by the sills and 80°N); the southern SPG (bounded by 45°N and the OSNAP line). Transects are as follows: East Greenland section (A); North east Labrador Sea Section (B); Newfoundland section (C). The latitude 45°N is highlighted by the black dashed line.

water mass transformation is greater north of OSNAP-E (eastern SPG section) than OSNAP-W (western SPG section; see Figure 1) (Desbruyères et al., 2019). This water mass transformation has been found to be a large contributor to the overturning in density space, even on decadal timescales (Josey et al., 2009; Marsh, 2000). These studies also found that about half the mean transformation (Chafik & Rossby, 2019) and most of the decadal variability (Desbruyères et al., 2019) actually occur in the Irminger Sea and Icelandic basin (between OSNAP-E and the ridge separating the North Atlantic from the GIN seas), rather than in the GIN seas itself.

Collectively, these recent studies call into question whether overturning in the Labrador Sea is relevant for the AMOC, with implications for the overall fidelity of climate models in representing the behavior of the North Atlantic. If climate models do not have the correct relationship between the AMOC and density anomalies in the Labrador Sea, can we trust them to adequately reproduce the AMOC and the decadal and centennial predictions/projections that rely on AMOC variability?

In order to begin to address these questions, we present the first direct comparison between OSNAP and a free-running coupled climate model of the kind used for climate projections. In section 3.1, we investigate whether the recent observations are well represented in this model. In section 3.2, we investigate whether this model behaves similarly to previous models. In section 3.3, we then test our hypothesis that the linkage between Labrador Sea densities and the AMOC in climate models is due to the impact of density transformation in the Irminger Sea on downstream Labrador Sea densities. A discussion and conclusions are presented in section 4.

2. Data and Methods

2.1. The Model

In this analysis we make use of preindustrial control simulations of the CMIP6 (6th Coupled Model Intercomparison Project) coupled climate model HadGEM3-GC3.1-MM (Menary et al., 2018; Williams et al., 2018). Interannually constant forcings appropriate for the year 1850 are used. The horizontal atmospheric resolution is approximately 60 km, and the ocean resolution is 0.25° latitude and longitude. Vertically, the atmosphere comprises 85 pressure levels and the ocean 75 depth levels. Atmosphere and ocean are coupled once per hour. The climate model also uses the JULES land surface (Walters et al., 2017) and CICE sea ice (Ridley et al., 2018) submodels. We also make brief comparisons to the lower resolution climate model counterpart: HadGEM3-GC3.1-LL. In this model version the horizontal resolution is reduced to approximately 135 km in the atmosphere and 1° in the ocean, typical of CMIP5.

2.2. The OSNAP Observations

OSNAP combines fixed current meter arrays, gliders, and hydrographic observations to estimate the temperature, salinity (density), and velocity across two transects in the subpolar gyre (see Figure 1). Different elements of the system use different deployment and retrieval schedules and the first synthesized results represent the 21 month period from August 2014 to April 2016 (Lozier et al., 2019). The data we use are quality-controlled, postprocessed, monthly mean profiles of the overturning in both density and depth space across these two sections along with the full, combined section.

2.3. Construction of OSNAP Stream Functions

To calculate the simulated overturning across the OSNAP section we first construct a line along vorticity points of the Arakawa C grid (Madec, 2008) that is as close as possible to the OSNAP observational locations. This allows velocities across the line to be extracted while preserving the total model transport across the line. Densities are regridded onto velocity points and the overturning is calculated by summing volume

transports along the line and finally summing cumulatively in either depth or density space as discussed in Lozier et al. (2019). For example, the overturning in density space is calculated as follows:

$$\Psi(\sigma) = -\int_{x_s}^{x_e}\int_{\sigma_{max}}^{\sigma_{min}} v(x,\sigma)d\sigma dx \quad (1)$$

where x_s and x_e denote the start and end of the horizontal section respectively, following a continuous set of grid points traveling from the westernmost to easternmost point. The σ_{max} and σ_{min} denote the maximum and minimum densities, respectively, and $v(x,\sigma)$ denotes the velocity perpendicular to the section (positive northward).

As also discussed in Lozier et al. (2019), the overturning stream functions across OSNAP-W and OSNAP-E show net transport through the sections. This leads to consideration of whether to apply a compensation term, and how this should be calculated and applied. The goal of such a compensation is to remove the impact of a net throughflow on the stream function, since this flow is not physically related to an actual overturning. In particular in the Labrador Sea the throughflow is associated with shallow, light waters flowing out of the Arctic. Removing a section mean transport could distort transports in the deep waters, particularly since the net throughflow across OSNAP-W in the model is 1.5 Sv, which is of a similar magnitude to the overturning transport. Hence, we apply no compensation and sum the transports from the deepest/densest levels to the shallowest/lightest levels allowing us to focus on the deep/dense overturning. This is done for both the model and the observations and is the same as in Lozier et al. (2019).

To create a time series of the overturning strength, we take the value of the stream functions at a fixed density/depth. Indices of the overturning for OSNAP-W, OSNAP-E, and the Full section are taken at $\sigma_\theta = (27.74, 27.66, 27.66)\,\mathrm{kg/m^3}$, respectively, in the model, denoted by horizontal lines in Figure 2b. For our calculation in depth space we use the fixed depth of $z = 1{,}000\,\mathrm{m}$ (supporting information). These indices are chosen to maximize the peaks in both OSNAP-W and OSNAP-E overturning cf. Figure 2b. We use fixed values rather than the maxima to avoid potential artifacts of aliasing switching in the density of the stream function maximum, particularly apparent in the OSNAP-W stream functions in density space (Figure 2b).

3. Results

3.1. OSNAP Section in Model and Observations.

3.1.1. Time Mean

In order to begin the reconciliation of the climate model paradigm and new OSNAP observations, we compare our model to these observations. The oceanic region of interest along with the names and locations of key features is shown in Figure 1. Unless otherwise stated, overturning is calculated in density (rather than depth) space. The structure, magnitude, and monthly variability of the stream functions across the OSNAP sections agree well with observations (Figures 2a and 2b; see section 2.3). Both highlight that the majority of the overturning occurs across the OSNAP-E section (eastern SPG), rather than OSNAP-W (the Labrador Sea), where there are comparatively small values. This is strikingly different to a recent comparison of ocean-only models with observations, in which those models significantly overestimate the magnitude of overturning at OSNAP-W (Li et al., 2019). It is not the result of model resolution as a lower resolution model counterpart is also able to reproduce the dominance of OSNAP-E (supporting information Figure S1). For reference, the raw time series of overturning at specific density levels are shown in supporting information Figure S2.

The overturning across OSNAP-E can be deconstructed by analysis of the simulated stream function further north across the overflow sills (Denmark Straits and Iceland-Faroe Ridge; supporting information Figure S3). The strong overturning seen at OSNAP-E is not present in the overturning across the sills, showing that the former must be a result of density transformation in the eastern SPG. The prominence of the eastern SPG (south of the sills) in the model is consistent with implied overturning stream functions calculated from observational estimates of surface buoyancy fluxes (Desbruyères et al., 2019) (see supporting information Figure S4 for an analysis of the simulated, implied density transformation due to surface buoyancy fluxes). The very dense transports in the overturning across the sills are not seen in transports across OSNAP-E suggesting that these waters have been made lighter by mixing with less dense waters, likely along the boundary currents.

The model also allows comparison with the AMOC further south. The mean AMOC at the southern boundary of the subpolar gyre (here chosen as 45°N) is remarkably similar to the mean overturning across the

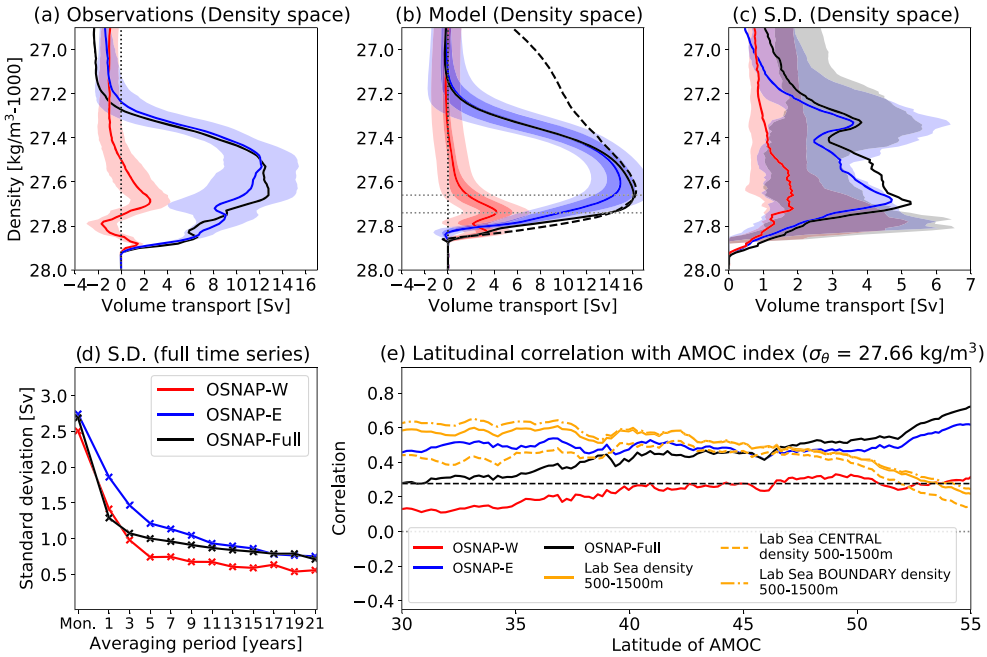

Figure 2. Observed (a) and modeled (b) overturning stream function in density space across the OSNAP sections, summed upward (red is OSNAP-W; blue is OSNAP-E; black is the total; see section 2.3). Light shading represents the monthly standard deviation and dark shading the annual standard deviation (model only). The black dashed line in (b) shows the profile of the AMOC at 45°N. (c) The full spread of standard deviations of 21 month portions of the simulated (shading) and observed (lines) overturning as a function of density across the OSNAP sections. (d) Standard deviation (full time series) of overturning at fixed densities from the model as a function of averaging period. (e) In phase correlation between the AMOC (σ_θ = 27.66 kg/m^3) and overturning across the OSNAP sections and area averaged density in the Labrador Sea (in the depth range 500–1,500 m; see Figure 1). Horizontal lines in panel (b) denote the densities used for the correlations displayed in panel (e) (σ_θ = 27.66 kg/m^3 for OSNAP-E/Full and σ_θ = 27.74 kg/m^3 for OSNAP-W). A 5 year running mean was applied prior to computing the correlations in panel (e). Also in panel e, the horizontal dashed line denotes significance at the 99% level for bootstrapped pseudo-data with the same mean, variance and first and second autocorrelation coefficients.

OSNAP line (16.3 Sv for the former; 16.1 Sv for the latter; see Figure 2b). Since volume transport across density bins in the lower limb is similar at the two locations, we infer then that there is little further transformation of the denser waters south of the OSNAP section. However, in the upper limb there is a difference, likely a reflection of light-to-dense transformation of very light, northward flowing, upper waters. For completeness, a similar analysis of the vertical overturning (i.e., in depth space) is provided in the supporting information (Figure S5).

3.1.2. Variability

In addition to representing well the time mean overturning, the model is also able to represent the observed magnitude of monthly variability across all of OSNAP-E, OSNAP-W, and the total OSNAP section (Figure 2c; see section 2.3). Here, the 300 years of model simulation are repeatedly subsampled to the length of the direct observations (21 months). The observed variability lies within the simulated range for both the OSNAP-E and OSNAP-W sections at all density levels. However, across the Full section between σ_θ = 27.5 kg/m^3 and σ_θ = 27.7 kg/m^3 the model appears to underestimate the variability. In both model and observations, the OSNAP-E section dominates the large monthly variability. Again, a broadly similar result is seen in the lower resolution model counterpart (supporting information Figure S1).

We also show the magnitude of variability across the OSNAP sections at various longer timescales (Figure 2d). On all timescales, the OSNAP-E section again dominates although OSNAP-W has a significant fraction of the variability. Furthermore, there is more variability in both sections in dense water overturning than in deep water overturning (cf. supporting information Figure S5). From here on, we focus on the time series created from the density level at/near the maximum of each time mean profile to investigate the interannual variability (see section 2.3).

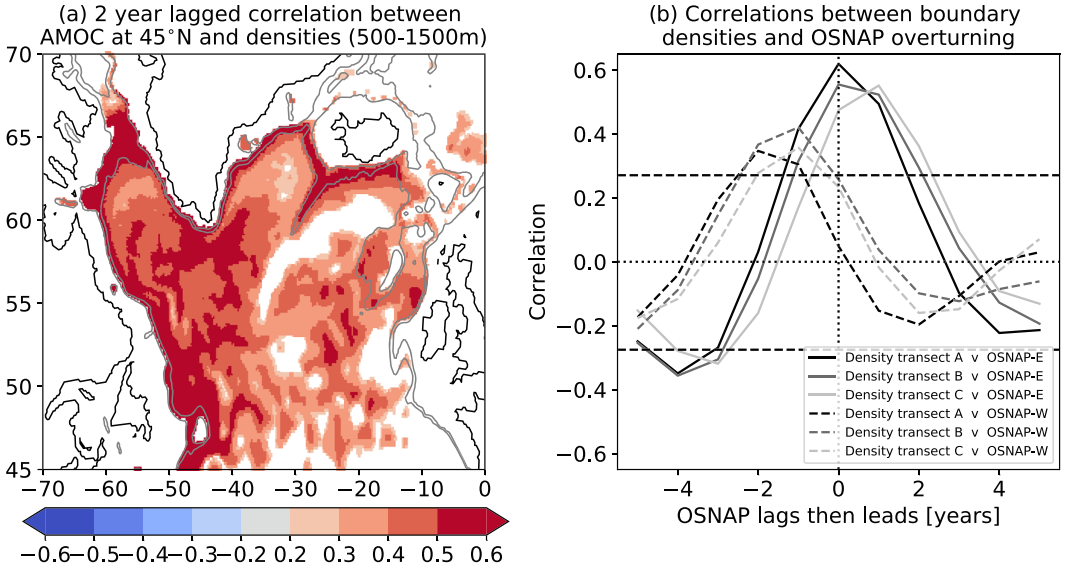

Figure 3. (a) Spatial map of the correlation between the AMOC at 45°N and middepth densities (depth range 500–1,500 m). AMOC lags by 2 years. (b) Lagged annual correlation between densities on the boundaries of the western SPG (see Figure 1) and time series of the overturning at OSNAP-E and OSNAP-W. Data not significant at the 99% level for bootstrapped pseudo-data with the same mean, variance, and first and second autocorrelation coefficients is masked in (a) and shown by horizontal dashed lines in (b).

3.2. This Model in the Context of Previous Models

We have shown good agreement between the time mean and monthly variability of the model and observations of the OSNAP section and that OSNAP-E dominates the overturning variability at all timescales. We now show that this model continues to conform to previous climate model-based paradigms.

Climate models have historically shown strong relationships between middepth densities in the western SPG and the lower latitude AMOC (Roberts et al., 2013; Robson et al., 2014, 2016). Such relationships between SPG densities and the AMOC persist in the current model (Figure 3a), notwithstanding the good agreement with OSNAP observations. The lower latitude AMOC has comparable correlations with densities in the western SPG and eastern SPG (Figure 3a), despite the preference (both observed and simulated) for dense water formation north of OSNAP-E (Figures 2a and 2b). Similar relationships are also seen in the lower resolution counterpart to the current model (supporting information Figure S1). As such, this model conforms to both the previous climate model paradigm (AMOC linked with western SPG densities) and new observations (that highlight the importance of overturning across OSNAP-E).

Also shown in Figure 2e is the relationship between the downstream AMOC and the OSNAP sections. The much stronger correlation between the AMOC and OSNAP-E (for all lags up to 5 years, not shown) is surprising given the comparable relationship between the AMOC and the densities in the western and eastern basins. As such, given the strong overturning across OSNAP-E (which correlates with the lower latitude AMOC) and the link between the lower latitude AMOC and middepth Labrador Sea densities, our hypothesis is that these Labrador Sea mid-depth density anomalies are formed by density transformation upstream in the Irminger Sea, with that density transformation also causing changes in the overturning at OSNAP-E. We explore this in section 3.3.

3.3. Linking the Irminger and Labrador Seas

To directly address the link between Irminger Sea surface forcing and the Labrador Sea middepth densities, we regress the integrated total surface buoyancy flux in various regions against these middepth (500–1,500 m) densities (Figure 4a). Even in the Labrador Sea region, nonlocal buoyancy forcing via the eastern SPG contributes significantly to the rate of change of subsurface densities. Directly comparing forcing in the Labrador Sea (local) and Irminger Sea (nonlocal; upstream), it is the Irminger Sea region that dominates this relationship. Furthermore, this link is dominated by the boundary regions (Figure 4b), while the contributions of local/nonlocal forcing to central Labrador Sea densities are weaker (Figure 4c). Nonetheless,

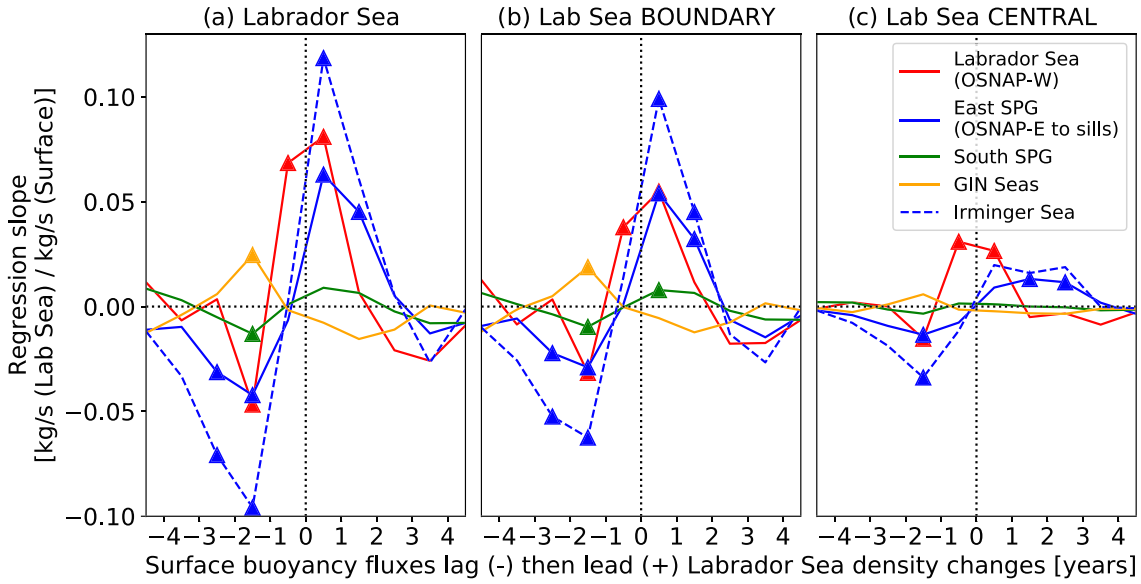

Figure 4. Regression slope coefficients between rate-of-change of volume integrated densities in the Labrador Sea (500–1,500 m) and area-integrated surface buoyancy fluxes in various regions. Lagged regressions are shown with density changes in the full Labrador Sea (a), Labrador Sea boundary (b), and central Labrador Sea (c). See Figure 1 for locations. Triangles denote when associated correlations are significant at the 99% level for bootstrapped pseudo-data with the same mean, variance and first and second autocorrelation coefficients.

there remains an important contribution of local (i.e., Labrador Sea) surface forcing of Labrador Sea densities, although this becomes relatively more important in the central Labrador Sea rather than along its boundary.

The importance of the boundaries is seen not only in their stronger relationship with buoyancy forcing but also as the strongest correlations between the AMOC and middepth densities in the western SPG appear at the boundaries (Figures 2e and 3a). To investigate the boundary density signal, we select transects within the narrow boundary current of the western subpolar gyre (Figure 1). We then correlate densities in these transects (defined as the cross-sectional mean density in the depth range 500–1,500 m) with the overturning across OSNAP-E and OSNAP-W, as previously defined. We find stronger correlations between all transects and the overturning across OSNAP-E than with the overturning across OSNAP-W (Figure 3b), particularly at lag 0.

The relative time lags between OSNAP-E and the transects is consistent with a picture of density anomalies propagating rapidly around the northwestern SPG: the total lag between Transects A and C is approximately 5 months using deseasoned monthly data, suggestive of a boundary wave process (Hodson & Sutton, 2012). The reduced correlations with OSNAP-W are also consistent with recent observational analyses showing that dense water formed across OSNAP-E enters and exits the Labrador Sea (OSNAP-W) with little density transformation (though with opposing contributions from the modification of temperature and salinity) (Zou et al., 2020). Nonetheless, while propagation around the Labrador basin is likely, the downstream increase in the correlations between AMOC and Labrador Sea densities (e.g., at 45°N; Figure 2e) suggests that such coherence may be more related to common atmospheric forcing (Zou et al., 2019) than to a continued boundary signal propagation (Hodson & Sutton, 2012).

4. Summary and Discussion

This is the first study to directly compare the OSNAP observations with a free-running coupled climate model of the type used in CMIP exercises. We have shown that the model well represents both the time mean and monthly variability across both OSNAP sections and that it captures the relative dominance of OSNAP-E over OSNAP-W. Previous modelling studies have focussed on the potential link between Labrador Sea (OSNAP-W) MLDs/convection and subsurface densities in the North Atlantic as a way to understand lower latitude AMOC variability (Robson et al., 2016). That relationship can also be seen in these simulations (Figure 3a), although we have confirmed that the relevant dense water formation can occur further east in

the SPG (OSNAP-E). Here, surface forcing in the Irminger Sea drives the formation of subsurface density anomalies that propagate into the Labrador Sea.

It should be noted that the model we have analyzed displays overly strong Labrador Sea convection (supporting information Figure S6), although the companion low-resolution model version displays the opposite bias and still agrees with the findings here, suggesting that these biases are not of first-order importance. Ultimately, in our model, both subsurface density anomalies in the Labrador Sea and overturning variability in the lower latitude AMOC are linked with surface forcing and subsurface density variability upstream in the Irminger Sea and overturning variability across OSNAP-E. As such, while a faithful representation of the overturning across OSNAP does not preclude a link between AMOC and Labrador Sea densities, this link and its relationship with local and upstream water mass transformation (in climate models) may need to be revisited.

In Figure 3 we noted the strong correlation between the lower latitude AMOC and boundary densities and investigated the propagation of these anomalies. In addition, density anomalies on the boundaries of the SPG may also be related to sinking in these regions. Sinking here is defined by the time mean vertical velocity and differs from deep convection which does not necessarily have a net vertical volume transport (Pickart & Spall, 2007). As noted previously, the time-mean vertical overturning (supporting information Figure S5) also demonstrates a dominant role for OSNAP-E rather than OSNAP-W (although there is also strong sinking south of the OSNAP line). A map of the absolute maximum vertical velocities (Figure 1, after Katsman et al., 2018) suggests that a large fraction of the vertical overturning occurs outside of the Labrador Sea around the boundaries of the SPG. Combined with the analysis above, these results demonstrate that the model can form dense water in appropriate regions, leading to increases in subsurface densities that drive sinking along the boundaries of the western SPG, in agreement with theoretical understanding (Katsman et al., 2018; Marshall & Schott, 1999; Pickart & Spall, 2007). However, the model emphasizes that these processes occur over a wider region than just the Labrador Sea and do not need to coincide geographically. In addition, the sensitivity of the link between overturning across the OSNAP section and the lower latitude AMOC to the vertical coordinate emphasizes that, when considering the North Atlantic SPG, a clear distinction between overturning in density and depth space should be made.

A region of particular importance in the link between SPG surface forcing and the downstream AMOC is the Irminger Sea (and Iceland basin), bounded to the south by the OSNAP-E line. As such, one possible reason for the prominence of the Labrador Sea in some previous modelling work may be the apparent coherence of variability in the Irminger and Labrador Seas—see, for example, Figure 7 of Roberts et al. (2013). We also find coherent variability in subsurface densities, but the surface forcing variability only shows a weak link (correlation of $r = 0.2$ on annual timescales) suggesting that the subsurface density similarities are not due to common surface forcing. Another possible reason for the prominence of the Labrador Sea in previous studies is a generous definition of the Labrador Sea that includes much of the Irminger Sea (Danabasoglu, 2008).

It is possible that oceanic resolution may be an important factor in correctly representing the sinking locations in the North Atlantic (Katsman et al., 2018) and in resolving eddies which may play important roles in mixing (Hirschi et al., 2020). We also note that a previous study found some forced ocean models had overly strong overturning across the OSNAP-W section (Li et al., 2019). As such, further analysis is required to understand the role of surface forcing, resolution and other model configurations on the location of density transformation, sinking and the representation of the AMOC.

In summary, recent, high-profile, direct observations of the overturning in the northern North Atlantic have called into question the fidelity of climate models in representing overturning in the North Atlantic. Based on myriad previous studies, the mostly model-derived paradigm had suggested that the Labrador Sea plays a primary role in modulating the annual/decadal variability in the AMOC. However, the recent observations have revealed a Labrador Sea that contributes weakly to the overturning in both the mean and variability across the northern SPG, and by inference the remainder of the North Atlantic. Here we have, for the first time, directly compared the observed overturning in the Labrador Sea to a coupled climate model and shown that agreement with the observations does not necessarily contradict results from previous model studies showing relationships between the downstream AMOC and subsurface Labrador Sea properties. Further work is required to directly understand how well other current generation coupled climate models compare to these new observations. Nonetheless, the results presented here allow us to have more confidence in the general ability of climate models to represent the overturning circulation and thus the potential

long-term effects of AMOC change. However, the causality in these relationships may be different than previously assumed.

Conflict of Interest

The authors declare that they have no competing financial interests.

Data Availability Statement

OSNAP data were collected and made freely available by the OSNAP (Overturning in the Subpolar North Atlantic Program) project and all the national programs that contribute to it (http://www.o-snap.org/observations/data/). The climate model simulations are available via the Earth System Grid Federation (ESGF) archive of Coupled Model Intercomparison Project 6 (CMIP6) data, for instance, on https://esgf-index1.ceda.ac.uk/projects/esgf-ceda/ website.

Acknowledgments
M. B. M. was supported by the EPICE project funded by the European Union's Horizon 2020 program, Grant Agreement 789445. L. C. J. was supported by the Joint U.K. BEIS/Defra Met Office Hadley Centre Climate Programme (GA01101). M. S. L. acknowledges the support from the Physical Oceanography Program of the National Science Foundation via Grant OCE-17-56223. Correspondence and requests for materials should be addressed to M. B. M.

References

Buckley, M. W., & Marshall, J. (2016). Observations, inferences, and mechanisms of the Atlantic Meridional Overturning Circulation: A review. *Reviews of Geophysics*, *54*, 5–63. https://doi.org/10.1002/2015RG000493

Chafik, L., & Rossby, T. (2019). Volume, heat, and freshwater divergences in the subpolar North Atlantic suggest the Nordic seas as key to the state of the meridional overturning circulation. *Geophysical Research Letters*, *46*, 4799–4808. https://doi.org/10.1029/2019GL082110

Danabasoglu, G. (2008). On multidecadal variability of the Atlantic meridional overturning circulation in the community climate system model version 3. *Journal of Climate*, *21*(21), 5524–5544.

Desbruyères, D. G., Mercier, H., Maze, G., & Daniault, N. (2019). Surface predictor of overturning circulation and heat content change in the subpolar North Atlantic. *Ocean Science*, *15*(3), 809–817.

Escudier, R., Mignot, J., & Swingedouw, D. (2013). A 20-year coupled ocean-sea ice-atmosphere variability mode in the North Atlantic in an AOGCM. *Climate Dynamics*, *40*(3–4), 619–636.

Gregory, J., Dixon, K., Stouffer, R., Weaver, A., Driesschaert, E., Eby, M., et al. (2005). A model intercomparison of changes in the Atlantic thermohaline circulation in response to increasing atmospheric CO_2 concentration. *Geophysical Research Letters*, *32*, L12703. https://doi.org/10.1029/2005GL023209

Guemas, V., & Salas-Mélia, D. (2008). Simulation of the Atlantic meridional overturning circulation in an atmosphere–ocean global coupled model. Part I: A mechanism governing the variability of ocean convection in a preindustrial experiment. *Climate Dynamics*, *31*(1), 29–48.

Heuzé, C. (2017). North Atlantic deep water formation and AMOC in CMIP5 models. *Ocean Science*, *13*(4), 609.

Hirschi, J. J.-M., Barnier, B., Bning, C., Biastoch, A., Blaker, A. T., Coward, A., et al. (2020). The Atlantic Meridional Overturning Circulation in high-resolution models. *Journal of Geophysical Research: Oceans*, *125*, e2019JC015522. https://doi.org/10.1029/2019JC015522

Hodson, D. L., & Sutton, R. T. (2012). The impact of resolution on the adjustment and decadal variability of the Atlantic meridional overturning circulation in a coupled climate model. *Climate Dynamics*, *39*(12), 3057–3073.

Jackson, L., Kahana, R., Graham, T., Ringer, M., Woollings, T., Mecking, J., & Wood, R. (2015). Global and European climate impacts of a slowdown of the AMOC in a high resolution GCM. *Climate Dynamics*, *45*(11–12), 3299–3316.

Josey, S. A., Grist, J. P., & Marsh, R. (2009). Estimates of meridional overturning circulation variability in the North Atlantic from surface density flux fields. *Journal of Geophysical Research*, *114*, C09022. https://doi.org/10.1029/2008JC005230

Katsman, C. A., Drijfhout, S., Dijkstra, H. A., & Spall, M. A. (2018). Sinking of dense North Atlantic waters in a global ocean model: Location and controls. *Journal of Geophysical Research: Oceans*, *123*, 3563–3576. https://doi.org/10.1029/2017JC013329

Li, F., Lozier, M. S., Danabasoglu, G., Holliday, N. P., Kwon, Y.-O., Romanou, A., et al. (2019). Local and downstream relationships between Labrador Sea Water volume and North Atlantic meridional overturning circulation variability. *Journal of Climate*, *32*(13), 3883–3898.

Lozier, M. S., Li, F., Bacon, S., Bahr, F., Bower, A. S., Cunningham, S. A., et al. (2019). A sea change in our view of overturning in the subpolar North Atlantic. *Science*, *363*(6426), 516–521.

Madec, G. (2008). NEMO ocean engine: Note du pole de modélisation, Institut Pierre-Simon Laplace (IPSL), France, No 27 ISSN No 1288-1619, available at: http://www.nemo-ocean.eu, Tech. Rep., IPSL LSCE, UVSQ, CEA CNRS, Unite Mixte, Bat 712, F-91191 Gif Sur Yvette, France.

Marsh, R. (2000). Recent variability of the North Atlantic thermohaline circulation inferred from surface heat and freshwater fluxes. *Journal of Climate*, *13*(18), 3239–3260.

Marshall, J., & Schott, F. (1999). Open-ocean convection: Observations, theory, and models. *Reviews of Geophysics*, *37*(1), 1–64.

Medhaug, I., Langehaug, H., Eldevik, T., Furevik, T., & Bentsen, M. (2012). Mechanisms for decadal scale variability in a simulated Atlantic meridional overturning circulation. *Climate Dynamics*, *39*(1–2), 77–93.

Menary, M. B., & Hermanson, L. (2018). Limits on determining the skill of North Atlantic Ocean decadal predictions. *Nature Communications*, *9*, 1694.

Menary, M. B., Hodson, D. L., Robson, J. I., Sutton, R. T., & Wood, R. A. (2015). A mechanism of internal decadal Atlantic ocean variability in a high-resolution coupled climate model. *Journal of Climate*, *28*(19), 7764–7785.

Menary, M. B., Kuhlbrodt, T., Ridley, J., Andrews, M. B., Dimdore-Miles, O. B., Deshayes, J., et al. (2018). Preindustrial control simulations with HadGEM3-GC3.1 for CMIP6. *Journal of Advances in Modeling Earth Systems*, *10*, 3049–3075. https://doi.org/10.1029/2018MS001495

Park, W., & Latif, M. (2010). Pacific and Atlantic multidecadal variability in the Kiel Climate Model. *Geophysical Research Letters*, *37*, L24702. https://doi.org/10.1029/2010GL045560

Pickart, R. S., & Spall, M. A. (2007). Impact of Labrador Sea convection on the North Atlantic meridional overturning circulation. *Journal of Physical Oceanography*, *37*(9), 2207–2227.

Rahmstorf, S., Feulner, G., Mann, M. E., Robinson, A., Rutherford, S., & Schaffernicht, E. J. (2015). Exceptional twentieth-century slowdown in Atlantic Ocean overturning circulation. *Nature Climate Change*, *5*(5), 475–480.
Ridley, J. K., Blockley, E. W., Keen, A. B., Rae, J. G., West, A. E., & Schroeder, D. (2018). The sea ice model component of HadGEM3-GC3.1. *Geoscientific Model Development*, *11*(2), 713–723.
Roberts, C. D., Garry, F. K., & Jackson, L. C. (2013). A multimodel study of sea surface temperature and subsurface density fingerprints of the Atlantic meridional overturning circulation. *Journal of Climate*, *26*(22), 9155–9174.
Robson, J., Hodson, D., Hawkins, E., & Sutton, R. (2014). Atlantic overturning in decline? *Nature Geoscience*, *7*(1), 2–3.
Robson, J., Ortega, P., & Sutton, R. (2016). A reversal of climatic trends in the North Atlantic since 2005. *Nature Geoscience*, *9*(7), 513–517.
Robson, J., Polo, I., Hodson, D. L., Stevens, D. P., & Shaffrey, L. C. (2018). Decadal prediction of the North Atlantic subpolar gyre in the HiGEM high-resolution climate model. *Climate Dynamics*, *50*(3–4), 921–937.
Stommel, H. (1961). Thermohaline convection with two stable regimes of flow. *Tellus*, *13*(2), 224–230.
Stouffer, R. J., Yin, J., Gregory, J., Dixon, K., Spelman, M., Hurlin, W., et al. (2006). Investigating the causes of the response of the thermohaline circulation to past and future climate changes. *Journal of Climate*, *19*(8), 1365–1387.
Thornalley, D. J., Oppo, D. W., Ortega, P., Robson, J. I., Brierley, C. M., Davis, R., et al. (2018). Anomalously weak Labrador Sea convection and Atlantic overturning during the past 150 years. *Nature*, *556*(7700), 227.
Walters, D., Boutle, I., Brooks, M., Thomas, M., Stratton, R., Vosper, S., et al. (2017). The Met Office unified model global atmosphere 6.0/6.1 and JULES global land 6.0/6.1 configurations. *Geoscientific Model Development*, *10*(4), 1487.
Williams, K., Copsey, D., Blockley, E., Bodas-Salcedo, A., Calvert, D., Comer, R., et al. (2018). The Met Office global coupled model 3.0 and 3.1 (GC3. 0 and GC3. 1) configurations. *Journal of Advances in Modeling Earth Systems*, *10*, 357–380. https://doi.org/10.1002/2017MS001115
Wood, R. A., Keen, A. B., Mitchell, J. F., & Gregory, J. M. (1999). Changing spatial structure of the thermohaline circulation in response to atmospheric CO2 forcing in a climate model. *Nature*, *399*(6736), 572–575.
Yashayaev, I., & Loder, J. W. (2016). Recurrent replenishment of Labrador Sea water and associated decadal-scale variability. *Journal of Geophysical Research: Oceans*, *121*, 8095–8114. https://doi.org/10.1002/2016JC012046
Zhang, L., & Wang, C. (2013). Multidecadal North Atlantic sea surface temperature and Atlantic meridional overturning circulation variability in CMIP5 historical simulations. *Journal of Geophysical Research: Oceans*, *118*, 5772–5791. https://doi.org/10.1002/jgrc.20390
Zou, S., Lozier, M. S., & Buckley, M. (2019). How is meridional coherence maintained in the lower limb of the Atlantic Meridional Overturning Circulation? *Geophysical Research Letters*, *46*, 244–252. https://doi.org/10.1029/2018GL080958
Zou, S., Lozier, M. S., Li, F., Abernathey, R., & Jackson, L. (2020). Density-compensated overturning in the Labrador Sea. *Nature Geoscience*, *13*, 121–126.

References From the Supporting Information

Griffies, S. M., Danabasoglu, G., Durack, P. J., Adcroft, A. J., Balaji, V., Boning, C. W., et al. (2016). OMIP contribution to CMIP6: Experimental and diagnostic protocol for the physical component of the Ocean Model Intercomparison Project. *Geoscientific Model Development*, *9*, 3231–3296.
Grist, J. P., Josey, S. A., & Marsh, R. (2012). Surface estimates of the Atlantic overturning in density space in an eddy-permitting ocean model. *Journal of Geophysical Research*, *117*, C06012. https://doi.org/10.1029/2011JC007752
Grist, J. P., Marsh, R., & Josey, S. A. (2009). On the relationship between the North Atlantic meridional overturning circulation and the surface-forced overturning streamfunction. *Journal of Climate*, *22*(19), 4989–5002.
Walin, G. (1982). On the relation between sea-surface heat flow and thermal circulation in the ocean. *Tellus*, *34*(2), 187–195.